Journal of Electrical Engineering, Vol. 75, No. 5, 2024, pp. 399-410

sciendo
PAPERS

A novel method based on PSO algorithm and ANN for magnetic flux density estimation near overhead transmission lines

Emir Turajlić, Adnan Mujezinović, Ajdin Alihodžić

This paper introduces a novel method that leverages artificial neural networks to estimate magnetic flux density in the proximity of overhead transmission lines. The proposed method utilizes an artificial neural network to estimate the parameters of a mathematical model that describes the magnetic flux density distribution along the lateral profile for various configurations of overhead transmission lines. The training target data is acquired using the particle swarm optimization algorithm. A performance comparison between the proposed method and the Biot-Savart law-based method is conducted using an extensive test dataset. The resulting coefficient of determination and mean square error values demonstrate the successful application of the proposed method for a range of different spatial arrangements of phase conductors. Furthermore, the performance of the proposed method is thoroughly assessed on multiple test cases. The practical relevance of the proposed method is highlighted by contrasting its results with the field measurements obtained in the proximity of a 400 kV overhead transmission line.

Keywords: multilayer perceptron, particle swarm optimization, magnetic flux density, overhead transmission lines

1 Introduction

Recent advancements in artificial intelligence have had a significant impact on data analysis, pattern recognition, predictive modeling and decision-making. Various artificial intelligence techniques have proven effective in addressing a wide range of different engineering challenges [1]. This paper utilizes artificial neural networks (ANNs) and the particle swarm optimization (PSO) algorithm to tackle the problem of estimating magnetic flux density values near overhead lines.

Due to escalating power demands and ongoing construction of high voltage overhead transmission lines (OHTL), there are growing concerns regarding the effects of electromagnetic pollution on living beings [2, 3]. Several international organizations have put forth guidelines and standards regarding occupational and general public exposure to magnetic fields [4-7]. Analyzing the magnetic flux density generated by overhead transmission lines is important in order to satisfy public health concerns and national regulations that require that such analysis is performed for existing and newly planned overhead lines. Over the years, a multitude of approaches and methods have emerged for determining the magnetic flux density near overhead lines. Since magnetic flux density measurements require time, equipment, and human resources, analytical and numerical techniques are commonly used to compute the magnetic flux density near overhead lines [8-13]. Recently, a range of ANN-based methods have emerged for estimating the magnetic flux density in the proximity of overhead lines [14-17]. Metaheuristic algorithms have also been applied to this research problem [2, 3, 18].

In [17], a method based on the cascade-forward neural network for estimation of electric and magnetic fields near high voltage overhead transmission line is considered. In [15], a typical 154 kV power transmission line in Turkey is studied and artificial neural network models are developed to predict electric and magnetic field values near the transmission line. In [15], the ANN models have only two input variables, the horizontal and vertical coordinates of the estimation point. In [16], the use of normalized radial basis function (NRBF) for determining the magnetic field near power transmission lines is outlined. The NRBF network in [16] has only two input variables which define the coordinates of the point where magnetic field intensity is estimated.

In this paper, a novel method for accurate estimation of magnetic flux density across various phase conductor configurations and for varying current intensity values is proposed. The proposed method adopts a significantly different approach to recently proposed ANN-based magnetic flux density estimation methods [14, 19]. Application of the ANN model in [14] is further examined in [20]. The methods in [14, 19] are developed to estimate magnetic flux density at a single point on the lateral profile. Hence, in order to appropriately describe the magnetic flux density distribution over the lateral profile for a given spatial arrangement of phase conductors, these methods need to independently evaluate the magnetic flux density estimate for each

Faculty of Electrical Engineering, University of Sarajevo, Sarajevo, Bosnia and Herzegovina
emir.turajlic@etf.unsa.ba, adnan.mujezinovic@etf.unsa.ba, ajdin.alihodzic@etf.unsa.ba

https://doi.org/10.2478/jee-2024-0048, Print (till 2015) ISSN 1335-3632, On-line ISSN 1339-309X

considered point along the lateral profile. The proposed method greatly simplifies the estimation of magnetic flux density distribution along the lateral profile for a given spatial arrangement of phase conductor. Instead of considering individual points along the lateral profile, the proposed method uses an ANN model to estimate the parameters of a mathematical model for magnetic flux density distribution along the lateral profile for a given phase conductor configuration. The ANN model is developed using an extensive training dataset. To ensure effective training, a particular attention is paid to input variable selection for the proposed ANN model. An additional novelty of the paper is related to the preparation of the training dataset. Specifically, the proposed method relies on the application of the PSO algorithm to obtain the ANN target data for various phase conductor configurations.

Section 2 presents the proposed method for magnetic flux density estimation. Section 3 presents the experimental results. The performance of the proposed method is assessed on a range of different phase conductor configurations. The results of the proposed method are compared to the Biot-Savart law-based method and the field measurements. Section 4 concludes the paper.

2 Proposed method for magnetic flux density estimation

The block diagram of the proposed method is presented in Fig. 1(a). This method is designed to accurately estimate magnetic flux density distribution for various spatial arrangements of overhead transmission line phase conductors and for different current intensity values. As depicted in Fig. 1(a), the magnetic flux density estimates are generated using the following mathematical model

$$\hat{B} = L_s \cdot e^{-N_{MLP} \cdot x^2} \tag{1}$$

where $\hat{B}$ denotes the magnetic flux density estimate generated at a point located 1 m above the ground surface and at a lateral distance of x meters from the central phase conductor. The mathematical model in Eqn. (1) is a two-coefficient version of the model presented in [2, 18]. This model is defined by linear coefficient L_s and nonlinear coefficient N_{MLP} values. In this paper, the proposed method evaluates the coefficients of the model in Eqn. (1) based on the parametric representation of the spatial layout of OHTL phase conductors and the current intensity value, whereas in the papers [2, 18], the coefficients of the model are obtained by fitting the field model to the observed field measurements.

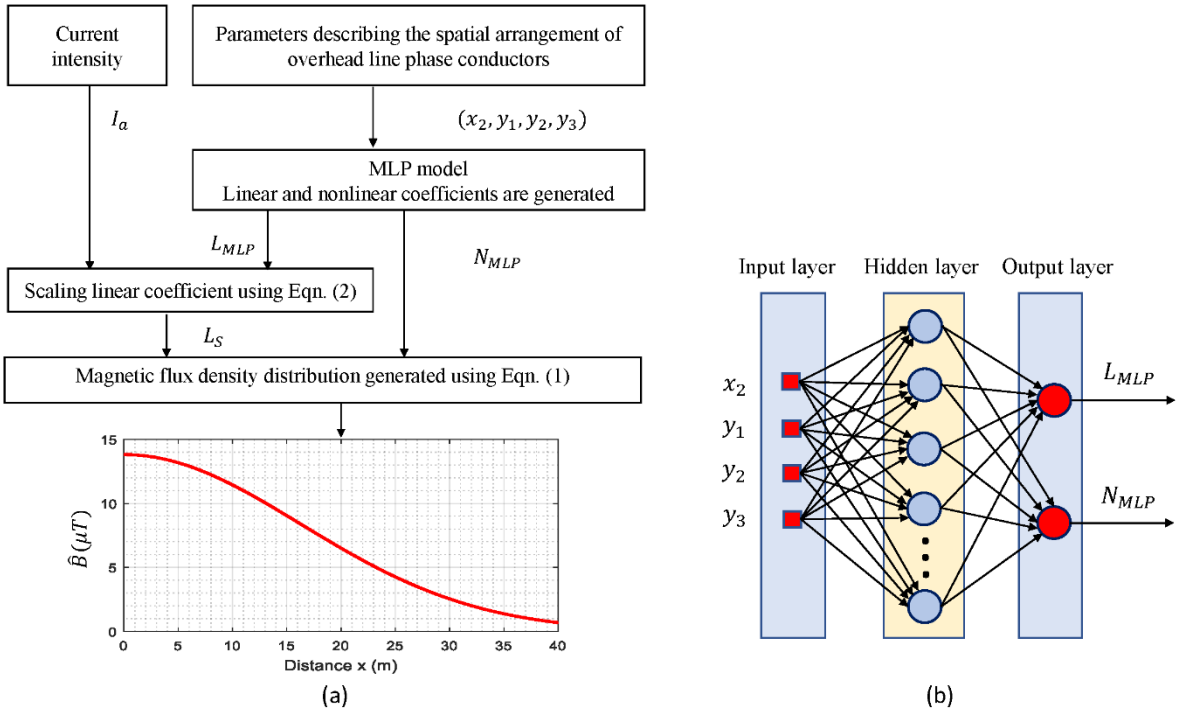

Fig. 1. (a) Proposed method for magnetic flux density estimation, (b) proposed multilayer perceptron (MLP) model

The proposed method generates the linear coefficient L_s and nonlinear coefficient N_{MLP} values without relying on field measurements. Instead, a multilayer perceptron (MLP) model is developed to evaluate the linear and nonlinear coefficient values of the function in Eqn. (1) for various spatial arrangements of OHTL phase conductors and for the reference current intensity value of $I_r = 100$ A. As shown in Fig. 1(a), in the first step of

the proposed method, a parametric representation for the spatial layout of OHTL phase conductors is established. This issue is discussed in more detail later on in this section of the paper.

For a given parametric representation of the spatial arrangement of overhead transmission line phase conductors, the MLP model produces two outputs, L_{MLP} and N_{MLP}. These values denote the linear and nonlinear coefficients in Eqn. (1) that are associated with the reference current intensity value. The reference current intensity value is used during the MLP training process. In instances when the transmission line current intensity differs from the reference current intensity value, $I_r = 100\ A$, the MLP output L_{MLP} is appropriately scaled to obtain the scaled linear coefficient value that is used in Eqn. (1). The scaled linear coefficient, L_s, is evaluated using the following equation:

$$L_s = L_{MLP} \cdot \frac{I_a}{I_r} \tag{2}$$

where I_a represents the actual transmission line current intensity value.

2.1 Multilayer perceptron

In this paper, a multilayer perceptron (MLP) is trained to estimate two parameters of the mathematical model that describes the magnetic flux density distribution over the entire lateral profile for a given OHTL phase conductor configuration and the reference current intensity value. Multilayer perceptron denotes a class of fully connected feedforward artificial neural networks. The considered MLP model consists of an input layer with 4 inputs, a hidden layer containing 60 neurons, and an output layer containing 2 neurons. Whilst other MLP architectures were considered, the selected MLP architecture provided the best results. Hyperbolic tangent is the chosen activation function for the hidden layer neurons [21]. The output of this nonlinear activation function ranges between –1 and +1 and its derivative has a higher magnitude around zero compared to the sigmoid function. Careful consideration is given to the selection of input variables for the proposed MLP model. Although magnetic flux density depends on the current intensity values, it was acknowledged that magnetic flux density is linearly proportional to current intensity. Rather than training the MLP model for a range of different current intensity values, the MLP model was developed and trained for the fixed reference current intensity value. Thus, the actual current intensity is not used as an MLP input parameter, but instead, its value is used to appropriately scale one of the MLP outputs. Hence, the only ANN inputs are parameters that define the spatial arrangement of the OHTL phase conductors. The spatial arrangement/layout of phase conductors refers to the specific positioning of three phase conductors within a two-dimensional space, and it is also referred to as a phase conductor configuration. The spatial arrangement of phase conductors can be represented by three coordinate pairs (x_1, y_1), (x_2, y_2) (x_3, y_3) as shown in Fig. 2.

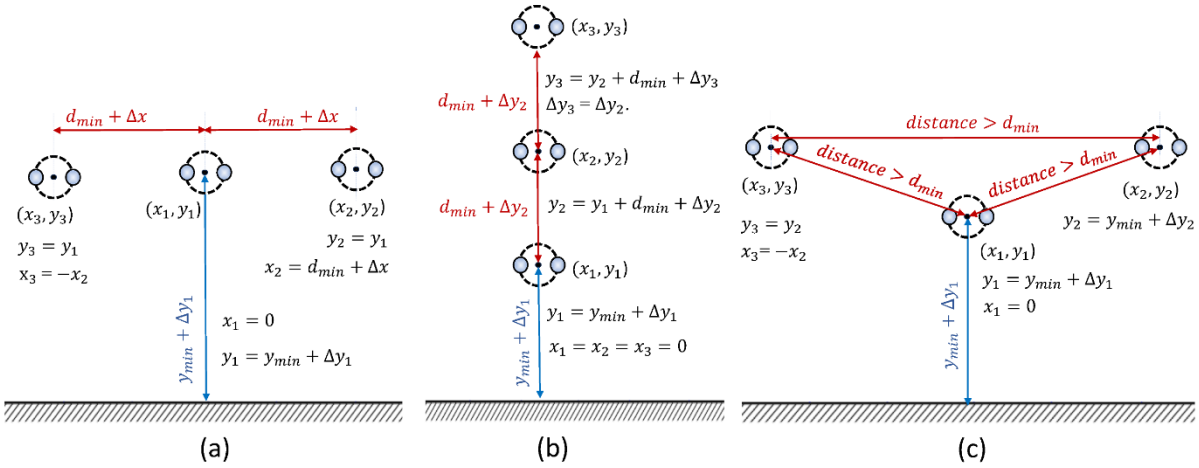

Fig. 2. Various types of OHTL configurations

Parametric representation of the spatial arrangement of phase conductors is based on a specific coordinate system that is adopted for this purpose. The central phase conductor is associated with the coordinate pair (x_1, y_1). In this coordinate system, the horizontal displacement of the central phase conductor from the coordinate origin is set to zero, whilst the *y*-axis denotes the vertical distance from the ground level. Furthermore, this paper considers the spatial arrangements of phase conductors where the two outer phase conductors are situated at an equal lateral distance from the central phase conductor. Thus, for all phase conductor configurations, the value of x_3 is

defined as $x_3 = -x_2$. Based on the adopted coordinate system, and the considered spatial relations between the phase conductors, the transmission line configuration can be defined by only four values, the height of the three phase conductors, y_1, y_2, y_3 and the lateral distance of one outer phase conductor from the central phase conductor, x_2. Based on these four parameters, the spatial arrangement of three phase conductors in a two-dimensional space can be defined as $(-x_2, y_3)$, $(0, y_1)$, (x_2, y_2). Thus, the MLP model has four inputs that define the spatial arrangement of overhead transmission line phase conductors, as depicted in Fig.1(b). The two outputs of the MLP model, namely L_{MLP}, and N_{MLP}, uniquely describe the magnetic flux density distribution over the lateral profile for a given spatial arrangement of OHTL phase conductors and the reference current intensity value.

The MLP training, validation, and testing are based on a dataset consisting of 120,000 examples of different spatial arrangements of overhead transmission line phase conductors. Scaled conjugate gradient (SCG) is the supervised learning algorithm that is selected for training the MLP model [22]. The main feature of the conjugate gradient algorithms is that they employ a search along conjugate directions, which generally leads to faster convergence than the search in the steepest descent directions [23]. The algorithm employs a step-size scaling mechanism [22]. A detailed description of the SCG algorithm is presented in [22].

The following steps are used to generate the dataset:

1. The first step is to generate 120,000 instances of different spatial arrangements of phase conductors. Parametric representations of different spatial arrangements of phase conductors, as previously discussed, denotes the MLP input data.
2. For each specific spatial arrangement of OHTL phase conductors, the Biot-Savart (BS) law-based method is employed to calculate the magnetic flux density values by sampling points along a lateral profile at varying distances from the central vertical line, covering a range from 0 to 40 meters, in increments of 1 meter.
3. For each phase conductor arrangement, the particle swarm optimization algorithm is employed to fit the mathematical model in Eqn. (3) to the magnetic flux density distribution calculated by BS method. The PSO algorithm is used to evaluate L_{PSO} and N_{PSO} coefficient values that minimize the objective function in Eqn. (9), and the results are used as the target data for that that specific spatial arrangement of phase conductors.

In the following subsections, a comprehensive elaboration of each of these steps is presented. The magnetic flux density distribution along the lateral profile is defined by equation

$$\hat{B}^{PSO} = L_{PSO} \cdot e^{-N_{PSO} \cdot x^2} \tag{3}$$

where $\hat{B}^{PSO}$ denotes the magnetic flux density distribution estimate generated at a point positioned 1 m above the ground level and at a lateral distance of x meters from the central phase conductor. This model is defined by the linear coefficient L_{PSO} and the nonlinear coefficient N_{PSO} values. There is a symmetry in the magnetic flux density values around the ordinate axis. Thus, the calculations by Biot-Savart law-based method [8] are carried out for non-negative x values. In addition, the BS calculations are based on the reference current intensity value, I_r, flowing through the phase conductors under the assumption of symmetrically loaded overhead transmission lines. The dataset is randomly partitioned into three distinct subsets: a training dataset consisting of 60% of the samples, a validation dataset with 20% of the samples, and a test dataset also containing 20% of the samples. Before training, the input and output data were normalized using the min–max method [24] to linearly transform the data to fall within a range [–1, 1].

2.2 Generating different spatial arrangements of phase conductors

The algorithm presented in [14] is used to generate 120,000 different spatial arrangements of OHTL phase conductors under certain constraints. Specifically, for the reference 400 kV overhead transmission lines, the minimal phase conductor height is set to $y_{min} = 6.44$ m, and the minimum permissible separation distance between any two phase conductors is set to $d_{min} = 7.4$ m. The minimal phase conductor height and the minimal distance between two adjacent phase conductors are prescribed by the relevant national documents that regulate overhead line design and construction. The values of these parameters can vary due to the number of different factors including the accessibility of the location, and electric and magnetic field exposure limitations. Thus, in this paper different spatial arrangements of phase conductors are considered in order to support the variety of possible phase conductor arrangements, and different limits regarding the minimal phase conductor height and minimal distance between two adjacent phase conductors. The procedure for generating different spatial arrangements of phase conductors is as follows. Each generated example of the spatial arrangement of phase conductors can be categorized into one of three configuration types. The first type of configuration, denoted as the horizontal configuration, is illustrated in Fig. 2(a). The height of the central phase conductors is derived using the expression

$y_1 = y_{min} + \Delta y_1$, where Δy_1, in this case, denotes a random number within the interval [0, 13.56]. The heights of the outer phase conductors are set equal to the height of the central phase conductor y_1, and thus $y_2 = y_3 = y_1$. As such, this type of configuration is principally characterized by the fact that all three phase conductors have the same height. As previously discussed, the central phase conductor is for all types of configurations located at $x_1 = 0$. The horizontal displacement of one outer phase conductor, x_2, is obtained using the following expression $x_2 = d_{min} + \Delta x$, where Δx denotes a random number within the interval [0, 7.6]. As previously discussed, the following relation holds true for all considered phase conductor configurations: $x_3 = -x_2$.

The second type of configuration, denoted as the vertical configuration, is presented in Fig. 2(b). In the vertical configuration, all three phase conductors are placed directly above each other, such that $x_1 = x_2 = x_3 = 0$. The height of the lowest phase conductor, y_1, is generated using the following expression $y_1 = y_{min} + \Delta y_1$, where Δy_1 denotes a random number within the interval [0, 2]. Thus, the minimum phase conductor height constraint is satisfied. The height of the phase conductor that is closer to the lowest phase conductor is derived from the following equation: $y_2 = y_1 + d_{min} + \Delta y_2$, where Δy_2 denotes a random number within the interval [0, 2]. Similarly, the height of the highest phase conductor is defined as $y_3 = y_2 + d_{min} + \Delta y_3$. Since in this type of configuration, the highest and the lowest phase conductors are positioned at equal distance from the central phase conductor, the value of Δy_3 is defined as $\Delta y_3 = \Delta y_2$. In this way, the imposed constraint regarding the minimal distance between any given pair of phase conductors is satisfied as well.

The third type of configuration, shown in Fig. 2(c), is characterized by the fact that the central phase conductor stands at a different height compared to the two outer phase conductors, whilst the heights of the two outer phase conductors remain equal. Thus, for this type of configuration, the following expression holds true: $y_2 = y_3 \neq y_1$. This configuration can be completely defined by three parameters y_1, y_2, and x_2. The height of the central phase conductors is derived using the expression $y_1 = y_{min} + \Delta y_1$, where Δy_1 denotes a random number within the interval [0, 13.56]. The value of parameter y_2 is obtained using a similar expression $y_2 = y_{min} + \Delta y_2$, where Δy_2 denotes a random number within the interval [0, 13.56]. Subsequently, the parameter x_2 is generated as a random number within the interval [0, 15] under the constraint that the minimal distance between any pair of phase conductors is d_{min}.

The dataset is generated in such a way that each type of OHTL phase conductor configuration is equally represented, i.e., 40,000 different examples of each configuration type are generated.

2.3 Particle swarm optimization algorithm

The particle swarm optimization algorithm is a widely used population-based stochastic optimization algorithm. The PSO algorithm is a well-established metaheuristic algorithm that has been successfully applied on a range of different problems. It only has few control parameters. In the PSO algorithm, each particle denotes a candidate solution to the optimization problem and its position constitutes a point in a *D*-dimensional solution space. Thus, a population (swarm) of *N* candidate solutions can be represented by matrix $\boldsymbol{X}$:

$$\boldsymbol{X} = \begin{bmatrix} x_{1,1} & x_{1,2} & \cdots & x_{1,D} \\ x_{2,1} & x_{2,2} & \cdots & x_{2,D} \\ \vdots & \vdots & \ddots & \vdots \\ x_{N,1} & x_{N,2} & \cdots & x_{N,D} \end{bmatrix} \tag{4}$$

The first step of the PSO algorithm is to randomly produce an initial population of candidate solutions. To ensure adequate search space coverage, the positions of PSO particles are initialized randomly within the search space [25], as in $x_{id}(0) \sim U(x_d^{min}, x_d^{max})$. Thus, for each i^{th} particle, the d^{th} component of the initial position vector is a uniformly distributed number between the lower bound, x_d^{min}, and upper bound, x_d^{max} of the d^{th} component. During the initialization phase of the PSO algorithm, the initial velocity of each particle is set to zero [25, 26]. In this paper, population size is set to 20 candidate solutions.

The particles move within a multi-dimensional search space with adjusted velocity in search of the optimal solution [27]. The velocity of each particle is dynamically modified based on the particle's personal best solution attained thus far and the historically best solution attained by any particle in the entire swarm [27]. At iteration t, the velocity vector of the i^{th} particle, denoted as $v_i = (v_{i1}, v_{i2}, \ldots, v_{iD})$, is updated using equation [27–29]

$$v_{id}(t+1) = \omega v_{id}(t) + c_1 r_1 \big(p_{id} - x_{id}(t)\big) + c_2 r_2 (p_{gd} - x_{id}(t)) \tag{5}$$

where r_1 and r_2 are two random numbers uniformly distributed between 0 and 1. The parameter ω denotes the inertia weight, while c_1 and c_2 represent the acceleration coefficients [26]. Furthermore, p_i represents the previous best position of the i^{th} particle according to its fitness values, whilst the historically best position attained by any member of the swarm is denoted as p_g. In Eqn. (5), p_{id} and p_{gd} denote the d^{th} component of p_i and p_g vectors, respectively. Note that in the global PSO version that is adopted in this paper, the best position previously attained by any member of the

swarm, p_g, is communicated to all the particles in the swarm. Furthermore, the initial personal best position of each i^{th} particle is set to the initial position of the i^{th} particle, whilst the initial best position of the entire swarm is set to the best initial position of all the particles in the swarm [25].

The choice of inertia weight value is important, as it affects the balance between global and local exploration and exploitation [29]. In this paper, inertia weight undergoes a linear reduction from $\omega_{init} = 0.9$ to $\omega_{fin} = 0.4$ as in [29, 30].

The cognitive acceleration coefficient, c_1, and social acceleration coefficient c_2, scale the stochastic acceleration terms that pull the individual particles in the direction of personal best (*pbest*), p_i, and global best (*gbest*) positions, p_g, respectively [27, 29]. Specifically, the cognitive acceleration coefficient c_1 controls the maximum step size of a particle toward the *pbest* position, whilst the social acceleration coefficient c_2 controls the maximum step size toward the *gbest* position [30]. In this paper, the acceleration coefficients are set to $c_1 = 2$ and $c_2 = 2$. These are commonly used values in the literature [29].

In this paper, velocity clamping is employed to limit the maximum velocity of each particle to prevent it from roaming excessively beyond the search space boundaries [25]. The d^{th} component of velocity vector for each particle is clamped to a range $[-v_d^{max}, v_d^{max}]$, where v_d^{max} denotes the predefined maximum velocity magnitude for the d^{th} component of the velocity vector. The velocity clamping is described by the following equation [25, 26, 31]:

$$v_{id}(t+1) = \begin{cases} v_d^{max}, & \text{if } v_{id}(t+1) > v_d^{max} \\ -v_d^{max}, & \text{if } v_{id}(t+1) < -v_d^{max} \\ v_{id}(t+1), & \text{otherwise} \end{cases} \quad (6)$$

where $v_{id}(t+1)$ denotes the d^{th} component of velocity vector associated with an i^{th} particle at iteration $(t+1)$ within the PSO algorithm. The v_d^{max} value defines velocity clamping. In literature, a common practice is to evaluate the parameter v_d^{max} using a function that depends on the search space boundaries [25, 26, 32]:

$$v_d^{max} = \delta(x_d^{max} - x_d^{min}) \quad (7)$$

where δ is a constant, whilst x_d^{max} and x_d^{min} denote the upper and lower boundaries of the search space in the d^{th} dimension, respectively. In this paper, the parameter δ is set to $\delta = 0.1$, as in [32]. For each particle, its velocity vector is used to update the position of that particle. The position vector $x_i = (x_{i1}, x_{i2}, \ldots, x_{iD})$ for the i^{th} particle is updated based on the following equation [27-29]:

$$x_{id}(t+1) = x_{id}(t) + v_{id}(t+1) \quad (8)$$

After the velocity and position of each particle have been updated, the fitness function of each particle is determined [25]. Following this, the personal best position of each particle is updated, and finally, the global best position is updated. Thus, if the updated position of a particle results in an improved fitness value compared to the particle's previous personal best, the particle's personal best position (*pbest*) is accordingly modified [25]. The updated global best position (*gbest*) denotes the best position attained by any particle in the swarm thus far. This process is repeated until a user-defined termination criterion is satisfied. In this paper, the maximum number of iterations is set to 50. After the algorithm is terminated, the best solution is returned. Table 1 presents the parameters of the PSO algorithm that are used in this paper.

Table 1. Parameters of the PSO algorithm

PSO parameters	value
Population size	$N = 20$
Cognitive acceleration coefficient	$c_1 = 2$
Social acceleration coefficient	$c_2 = 2$
Initial inertia weight value	$\omega_{init} = 0.9$
Final inertia weight value	$\omega_{fin} = 0.4$
Parameter δ	$\delta = 0.1$
Maximum number of iterations	$t_{max} = 50$
Lower bounds of the search space	$x^{min} = (0, 0)$
Upper bounds of the search space	$x^{max} = (15, 0.1)$

The PSO algorithm is employed to obtain the target data for the MLP training dataset. For each considered spatial arrangement of phase conductors and the reference current intensity value, I_r, the Biot-Savart law-based method is used to calculate the magnetic flux density for different points on the lateral profile. Subsequently, PSO algorithm is applied to fit the mathematical model in Eqn. (3) to the data obtained by the Biot-Savart law-based method.

Specifically, for a given spatial arrangement of OHTL phase conductors, the PSO algorithm is used to evaluate the linear and nonlinear coefficient values $\{\hat{L}_{PSO}, \hat{N}_{PSO}\}$ that minimize the following objective function:

$$f(L_{PSO}, N_{PSO}) = \frac{1}{T}\sum_{x=0}^{T-1}\left(B_x^{BS} - \hat{B}_x^{PSO}(L_{PSO}, N_{PSO})\right)^2 \quad (9)$$

where B_x^{BS} and $\hat{B}_x^{PSO}$ denote the magnetic flux density values evaluated at a point positioned 1 m above the ground level and at a lateral distance of x meters from the central phase conductor by BS method and the function in Eqn. (3), respectively. In each case, a total of $T = 41$ different points along the lateral profile were considered. For a specific layout of phase conductors, shown in Fig. 3(a), the results of minimizing the function in Eqn. (9) using the PSO algorithm are presented in Fig. 3(b). The obtained model parameters are $\hat{L}_{PSO}$ = 1.1816 μT and $\hat{N}_{PSO}$ = 0.00101. This example demonstrates how MLP training data is formed. For a given spatial arrangement of phase conductors, the MLP input vector is (x_2, y_1, y_2, y_3) and the targets vector is $(\hat{L}_{PSO}, \hat{N}_{PSO})$.

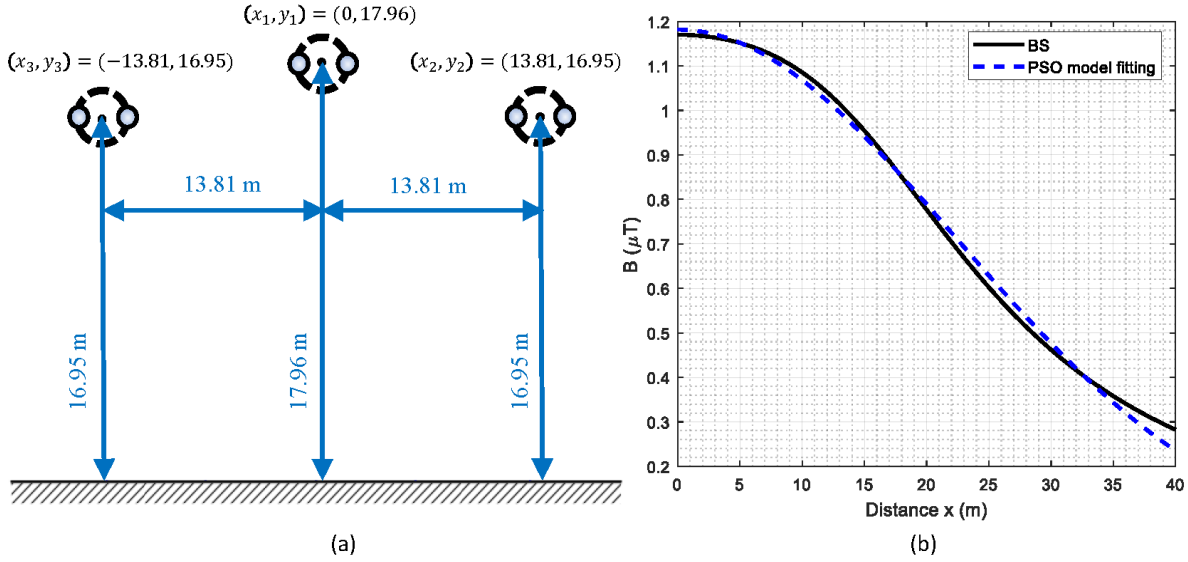

Fig. 3. (a) Spatial arrangement of phase-conductors (b) The magnetic flux density calculated using the BS method and the PSO-based fitting results

3 Experimental analysis

The performance of the proposed method for the estimation of magnetic flux density distribution along the lateral profile is compared to the Biot-Savart law-based method and field measurement results. The performance of the proposed method is compared to the BS method on a large test dataset and on four specific test cases its performance is analyzed in detail.

3.1 Comparative analysis with Biot-Savart law-based method

In the first experiment, the performance of the proposed PSO-ANN method is compared to the BS method on four test cases. Each test case is characterized by a specific phase conductor configuration and the current intensity value. The considered phase conductor configurations are presented in Fig. 4. The first two examples, shown in Fig. 4(a) and Fig. 4(b), correspond to the horizontal and vertical phase conductor configurations, respectively. The remaining two examples belong to the third phase conductor configuration type. In the example presented in Fig. 4(c), the central phase conductor is positioned at a greater height than the outer phase conductors, whereas in the example, shown in Fig. 4(d), the outer phase conductors are placed higher than the central phase conductor. For each considered test case, different current intensity values are used. For the test cases corresponding to the horizontal and vertical phase conductor configurations, the currents are set to I_a= 400 A and I_a = 600 A, respectively. On the other hand, for the test cases corresponding to the phase conductor configurations presented in Fig. 4(c) and Fig. 4(d), the currents are set to I_a= 800 A and I_a= 1000 A, respectively.

For each test case, the results obtained by the proposed method and the Biot-Savart law-based method are shown in Fig. 5. Furthermore, the performance of the proposed method is compared to the results obtained when the function in Eqn. (3) is fitted to the magnetic flux density distribution calculated by the Biot-Savart law-based method. PSO algorithm is employed to determine the coefficients of the function in Eqn. (3) by minimizing the objective function in Eqn. (9).

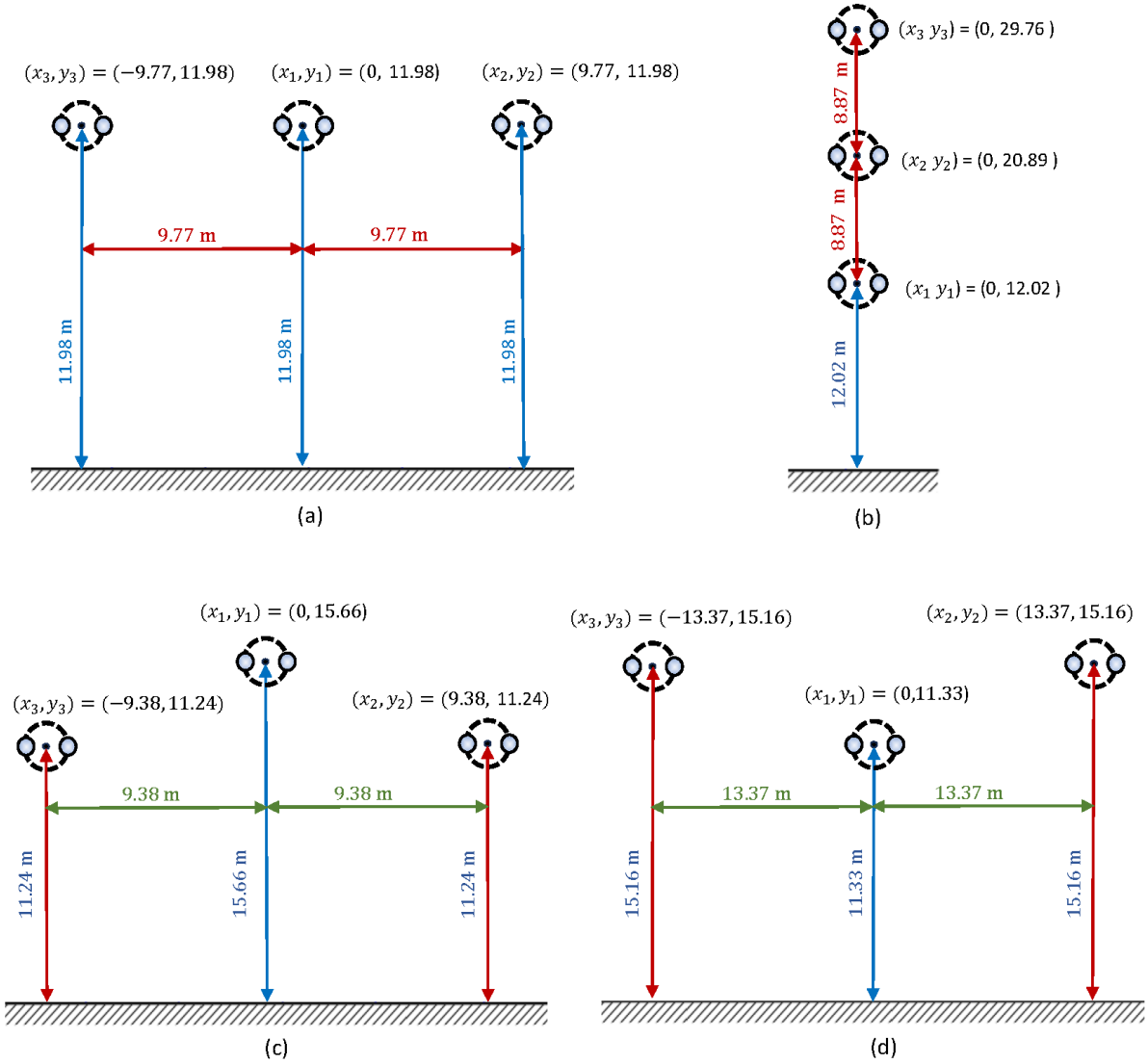

Fig. 4. Spatial arrangement of phase-conductors corresponding to four different test cases

Table 2. Linear and nonlinear coefficient values for different overhead line examples

Phase conductor configuration	Proposed method		Fitting results by PSO	
	Coefficient L_s (μT)	Coefficient N_{MLP}	Coefficient $\hat{L}_{PSO}$ (μT)	Coefficient $\hat{N}_{PSO}$
Example in Fig. 4(a)	6.9667	0.00191	6.9633	0.00191
Example in Fig. 4(b)	5.3362	0.00175	5.3603	0.00175
Example in Fig.4(c)	13.7891	0.00190	13.8235	0.00189
Example in Fig. 4(d)	16.4887	0.00136	16.4628	0.00136

In order to evaluated how closely the results of the proposed method approximate the results obtained by the BS method, the coefficient of determination (R^2) and mean square error (*MSE*) are evaluated for each of the four analyzed phase conductor arrangements. The *MSE* and R^2 are defined as follows:

$$MSE = \frac{1}{M}\sum_{\mathrm{i}=1}^{M}\left(B_i^{BS} - \hat{B}_i\right)^2 \tag{10}$$

$$R^2 = 1 - \frac{\sum_{\mathrm{i}=1}^{M}\left(B_i^{BS} - \hat{B}_i\right)^2}{\sum_{\mathrm{i}=1}^{M}\left(B_i^{BS} - \bar{B}^{BS}\right)^2} \tag{11}$$

Here, B_i^{BS} denotes the i^{th} magnetic flux density value calculated by BS method, whereas $\bar{B}^{BS}$ denotes the average value of all results calculated using the BS method. The $\hat{B}_i$ denotes the i^{th} magnetic flux density value estimated using the proposed method, and *M* represents the total number of considered samples.

For the phase conductor configurations in Fig. 4 (a)-(d), the *MSE* results are 0.067×10^{-12} T^2, 0.158×10^{-12} T^2, 0.265×10^{-12} T^2, 0.217×10^{-12} T^2, respectively. For the phase conductor configurations in Fig. 4 (a)-(d) the obtained R^2 results are 0.987, 0.943, 0.987, 0.991, respectively.

Figure 5 demonstrates that the proposed PSO-ANN based method is able to generate magnetic flux density estimates that at numerous instances reasonably well approximate the magnetic flux density values obtained by the BS method. However, there are some instances where more notable differences between the results obtained by these two methods can be observed. It is important to emphasize that the proposed method describes the magnetic flux distribution over the lateral profile using a mathematical model that is defined with only two parameters and thus, the proposed method is not always able to very closely approximate BS results at all instances. However, it should be emphasized that in all four cases, the results of the proposed method very closely approximate the results that are obtained when this mathematical model is directly fitted to the observed BS values.

In addition, the results of the proposed method are very similar to the results attained by directly fitting the function in Eqn. (3) to the magnetic flux density distribution obtained by the BS method. It is important to emphasize that the proposed method uses only five input parameters and relies on the use of the proposed ANN model to estimate linear and non-linear coefficient values, whereas PSO-based model fitting approach requires that the magnetic flux density distribution over the lateral profile is previously calculated by the BS method.

As shown in Fig. 5, the difference in the magnetic flux density estimates between the BS method and the proposed method are most notable for the case of vertical arrangement of phase conductors in Fig. 4(b). The observed discrepancies between the results obtained by the proposed method and the BS method, Fig. 5(b), can be attributed to the inability of the considered two-parameter mathematical model to describe the shape of the magnetic flux density distribution over lateral profile that is obtained by the BS method. Even when the considered mathematical model is directly fitted to the obtained BS results, the obtained results are very similar to those that were obtained by the proposed method.

Table 2 shows the linear and non-linear coefficient values estimated by the proposed method and the PSO-based model fitting approach for each test case. There is very little discrepancy in the coefficient values between the two methods. Given the intrinsic nature of the model utilized to describe the magnetic flux density distribution along the lateral profile, it is easy to consider how the obtained coefficient values affect the resulting magnetic flux density distribution.

In the next experiment, the performance of the proposed magnetic flux density estimation method is evaluated on a large test dataset. The performance of the proposed method is assessed using the following metrics: the mean squared error (*MSE*) and the coefficient of determination (R^2), defined in Eqn. (10) and Eqn. (11), respectively. The test dataset contains 984,000 magnetic flux density data points. Specifically, the dataset represents 24,000 different spatial arrangements of phase conductors. $I_r = 100$ A is assumed. For each spatial arrangement of phase conductors, 41 different locations over the lateral profile are considered, from x = 0 m to x = 40 m, in increments of 1 m.

Based on the test dataset with M = 984,000 data points, the following coefficient of determination and mean square error values are attained: R^2 = 0.9722 and *MSE* = 0.0124×10^{-12} T^2. These results highlight the versatility of the proposed method, showcasing its applicability across a variety of different spatial arrangements of phase conductors.

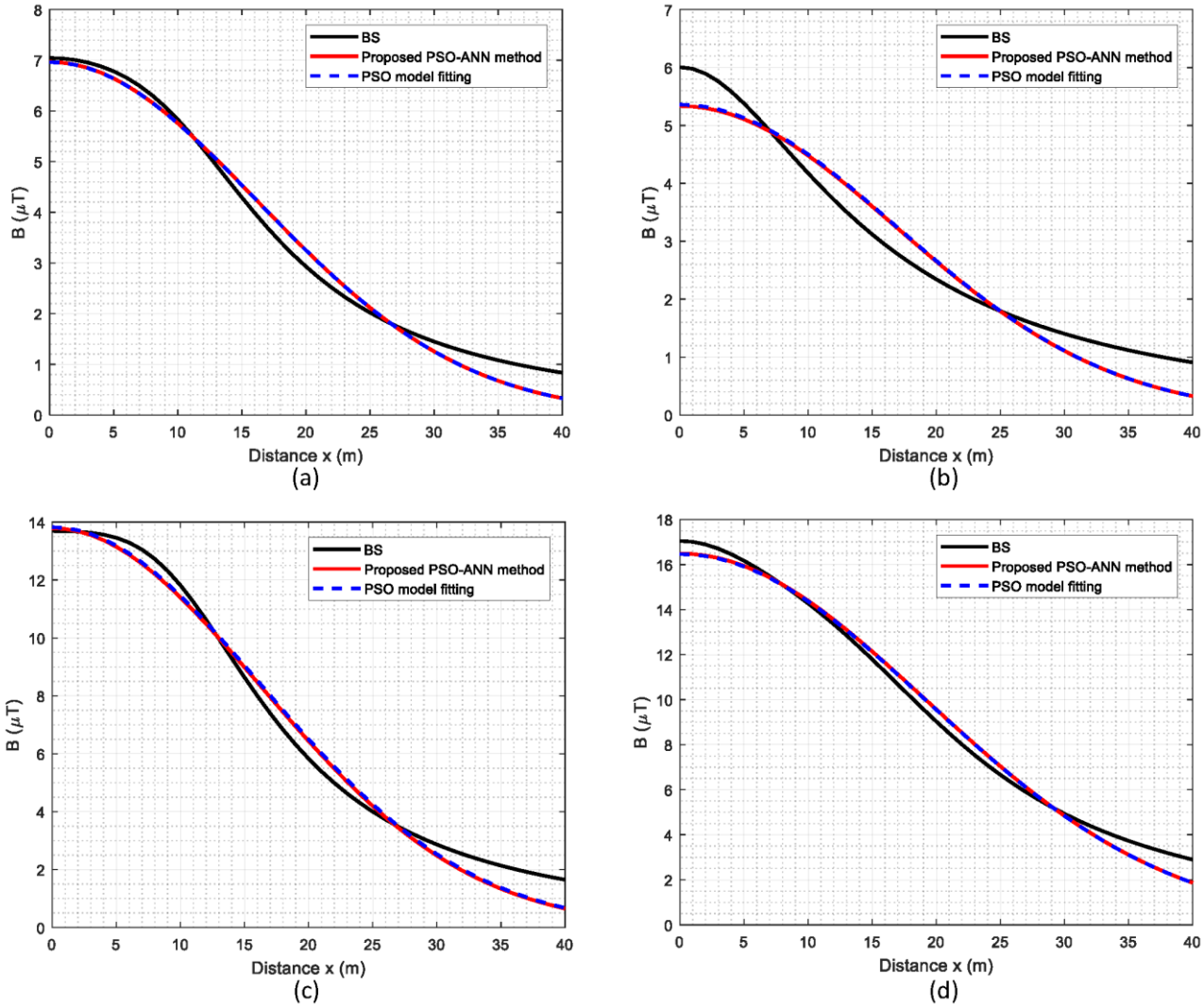

Fig. 5. The results of magnetic flux density estimation using the proposed PSO-ANN method, Biot-Savart law-based (BS) method and PSO-based model fitting

3.2 Comparative analysis with field measurement results

In this section, a real 400 kV overhead transmission line connecting substation (SS) Sarajevo 10 to substation Sarajevo 20 is considered. This overhead line has a horizontal configuration of phase conductors. A handheld cable height meter instrument, Suparule model 600 is used to measure the height of each phase conductor. The spatial arrangement of phase conductors is presented in Fig. 6(a). Phase current intensity of I = 86.88 A serves as the common input parameter for both the proposed method and BS method. Current intensity value is obtained from SCADA system. On the other hand, the instrument Narda ELT - 400 with a 3D probe is used to obtain the magnetic flux density measurements along the lateral profile 1 m above the ground surface.

The field measurement results are presented in Fig. 6(b) along with the results determined by the BS method and the proposed method.

The magnetic flux density measurements presented in Fig. 6(b) are performed at 26 points on the lateral profile, that are 1 m apart and 1 m above ground level. Measurements are performed at a location in the suburban area, where the terrain can be considered as approximately flat with some minor local unevenness. The RMS value of magnetic flux density is measured. The measurement duration for one point was about 20 seconds. It should be noted, that even in the short amounts of time, a significant overhead line phase current intensity changes can occur. It is important to stress that the results obtained by the BS method are calculated using the exact phase conductor heights as shown in Fig. 6(a). Conversely, the proposed method for

magnetic flux density estimation assumed a perfectly horizontal spatial arrangement of phase conductors. Thus, the height of each phase conductor is set to the average value of all three phase conductors, thus h = 8.74 m. In this case, the proposed method obtained the following linear and non-linear coefficient values: L_s = 2.4159 μT and N_{MLP} = 0.00237.

Figure 6(b) demonstrates that the results of the proposed method closely approximate the field measurements and the results calculated by the BS method. Numerous instances can be observed where the magnetic flux density values derived from the proposed method are closer to the magnetic field measurements than the results of the BS method. The fact that current intensity varies during the time interval when the field measurements are performed can explain some of the observed discrepancies between the field measurements and the results obtained by the proposed method.

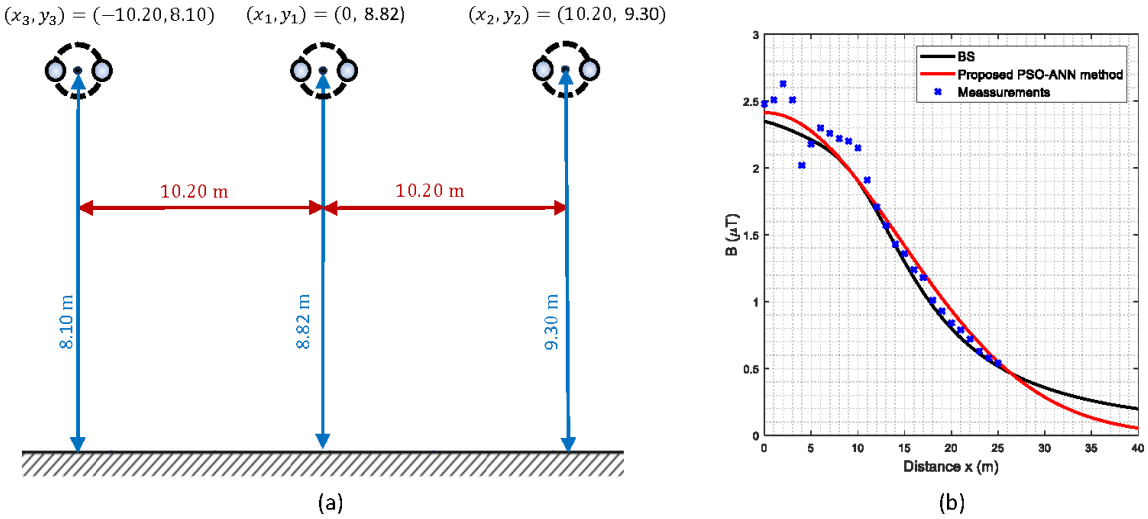

Fig. 6. Overhead transmission line SS Sarajevo 10 - SS Sarajevo 20: (a) Phase conductor configuration, (b) Magnetic flux density distributions

4 Conclusion

This paper presents a novel method based on particle swarm optimization and artificial neural networks for magnetic flux density estimation in the proximity of overhead transmission lines. The ANN model is trained using the scaled conjugate gradient algorithm to estimate the parameters of a mathematical model that describes the magnetic flux density distribution along the entire lateral profile for a range of different overhead transmission line configurations. To enable effective training of the ANN model, a specific emphasis is placed on selecting a small number of ANN input variables. The ANN model has only four inputs that define the spatial layout of phase conductors. For each considered phase conductor configuration in the training dataset, the particle swarm optimization algorithm is utilized to derive the training target data. The performance of the proposed method is compared to the Biot-Savart law-based method on a large test dataset. In addition, four test cases corresponding to different spatial arrangements of phase conductors and current intensity values have been examined in detail. The paper also examined a real 400 kV overhead transmission line, and a comparison was made between the results derived from the proposed method and the field measurements. The presented results showcase the successful application of the proposed method in estimating the magnetic flux density distribution across various phase conductor configurations and different current intensity values. The applications of the proposed method are constrained to the specific types of phase conductor configurations that were considered in this paper.

References

[1] O. I. Abiodun, A. Jantan, A. E. Omolara, K. V. Dada, N. A. Mohamed, and H. Arshad, "State-of-the-art in artificial neural network applications: A survey," *Heliyon*, vol. 4, no. 11, 2018.

[2] F. Muñoz, J. A. Aguado, F. Martín, J. J. López, A. Rodríguez, J. B. García, A. R. Treitero, and R. Molina, "An intelligent computing technique to estimate the magnetic field generated by overhead transmission lines using a hybrid GA-Sx algorithm," *International Journal of Electrical Power & Energy Systems*, vol. *53*, pp. 43-53, 2013.

[3] W. OuYang, J. Zhang, J. Hu, W. Lv, and D. Wang, "PSO/DE combined with simulation current method for the magnetic field under transmission lines in 3D calculation model," *Measurement and Control*, vol. 55, no. 9-10, pp. 1097-1109, 2022.

[4] IEEE, "IEEE Standard for Safety Levels with Respect to Human Exposure to Electric, Magnetic, and Electromagnetic Fields, 0 Hz to 300 GHz," *IEEE Std C95.1-2019 (Revision of IEEE Std C95.1-2005/ Incorporates IEEE Std C95.1-2019/Cor 1-2019)*, pp. 1-312, 2019.

[5] International Commission on Non-Ionizing Radiation Protection, "Guidelines for limiting exposure to time-varying electric and magnetic fields (1 Hz to 100 kHz)," *Health physics*, vol. 99, no. 6, pp. 818-836, 2010.

[6] Council of the European Union, "Council Recommendation of 12 July 1999 on the limitation of exposure of the general public to electromagnetic fields (0 Hz to 300 GHz) (1999/519/EC)," *Official Journal of the European Communities L*, vol 199, 1999.

[7] European Parliament, "Directive 2013/35/EU of the European Parliament and of the Council of 26 June 2013 on the minimum health and safety requirements regarding the exposure of workers to the risks arising from physical agents (electromagnetic fields) (20th individual Directive within the meaning of Article 16(1) of Directive 89/391/EEC) and repealing Directive 2004/40/EC," *Official Journal of the European Union L*, vol. 179, 2013.

[8] A. Geri, A. Locatelli, and G. M. Veca, "Magnetic fields generated by power lines," *IEEE Transactions on Magnetics*, vol. 31, no. 3, pp. 1508-1511, 1995.

[9] T. Modric, S. Vujević, and D. Lovrić, "3D computation of the power lines magnetic field," *Progress In Electromagnetics Research M*, vol. 41, pp. 1-9, 2015.

[10] G. Filippopoulos and D. Tsanakas, "Analytical calculation of the magnetic field produced by electric power lines," *IEEE Transactions on Power Delivery*, vol. 20, no. 2, pp. 1474-1482, 2005.

[11] J. B. Faria and M. E. Almeida, "Accurate calculation of magnetic-field intensity due to overhead power lines with or without mitigation loops with or without capacitor compensation," *IEEE Transactions on Power Delivery*, vol. 22, no. 2, pp. 951-959, 2007.

[12] K. Hameyer, R. Mertens, and R. Belmans, "Numerical methods to evaluate the electromagnetic fields below overhead transmission lines and their measurement," *Proceedings of First International Caracas Conference on Devices, Circuits and Systems*, pp. 32-36, 1995.

[13] I. Boukabou and N. Kaabouch, "Electric and magnetic fields analysis of the safety distance for UAV inspection around extra-high voltage transmission lines," *Drones*, vol. 8, no. 2, p. 47, 2024.

[14] A. Alihodzic, A. Mujezinovic, and E. Turajlic, "Electric and magnetic field estimation under overhead transmission lines using artificial neural networks," *IEEE Access*, vol. 9, pp. 105876-105891, 2021.

[15] H. F. Carlak, Ş. Özen, and S. Bilgin, "Low-frequency exposure analysis using electric and magnetic field measurements and predictions in the proximity of power transmission lines in urban areas," *Turkish Journal of Electrical Engineering and Computer Sciences*, vol. 25, no. 5, pp. 3994-4005, 2017.

[16] V. Ranković and J. Radulović, "Prediction of magnetic field near power lines by normalized radial basis function network," *Advances in Engineering Software*, vol. 42, no. 11, pp. 934-938, 2011.

[17] S. Alipour Bonab, W. Song, and M. Yazdani-Asrami, "A new intelligent estimation method based on the cascade-forward neural network for the electric and magnetic fields in the vicinity of the high voltage overhead transmission lines," *Applied Sciences*, vol. 13, no. 20, p. 11180, 2023.

[18] R. Gallego-Martínez, F. J., Muñoz-Gutiérrez, and A. Rodríguez-Gómez, "Trajectory optimization for exposure to minimal electromagnetic pollution using genetic algorithms approach: A case study," *Expert Systems with Applications*, vol. 207, p. 118088, 2022.

[19] A. Mujezinovic, E. Turajlic, A. Alihodzic, N. Dautbasic, and M. M. Dedovic, "Novel method for magnetic flux density estimation in the vicinity of multi-circuit overhead transmission lines," *IEEE Access*, vol. 10, pp. 18169-18181, 2022.

[20] A. Alihodzic, E. Turajlic, and A. Mujezinovic, "Machine learning model for electric and magnetic fields estimation in the proximity of overhead transmission lines," *2021 29th Telecommunications Forum (TELFOR)*, pp. 1-4, 2021.

[21] A. D. Rasamoelina, F. Adjailia, and P. Sinčák, "A review of activation function for artificial neural network," *2020 IEEE 18th World Symposium on Applied Machine Intelligence and Informatics (SAMI)*, pp. 281-286, 2020.

[22] M. F. Møller, "A scaled conjugate gradient algorithm for fast supervised learning," *Neural networks*, vol. 6, no. 4, pp. 525-533, 1993.

[23] D. Ö. Faruk, "A hybrid neural network and ARIMA model for water quality time series prediction," *Engineering applications of artificial intelligence*, vol. 23, no. 4, pp. 586-594, 2010.

[24] M. Tahan, M. Muhammad, and Z. A. Abdul Karim, "A multi-nets ANN model for real-time performance-based automatic fault diagnosis of industrial gas turbine engines," *Journal of the Brazilian Society of Mechanical Sciences and Engineering*, vol. 39, pp. 2865-2876, 2017.

[25] F. Marini and B. Walczak, "Particle swarm optimization (PSO). A tutorial," *Chemometrics and Intelligent Laboratory Systems*, vol. 149, pp. 153-165, 2015.

[26] E. T. Oldewage, A. P. Engelbrecht, and C. W. Cleghorn, "The merits of velocity clamping particle swarm optimisation in high dimensional spaces," *2017 IEEE Symposium Series on Computational Intelligence (SSCI)*, pp. 1-8, 2017.

[27] A. Rezaee Jordehi and J. Jasni, "Parameter selection in particle swarm optimisation: a survey," *Journal of Experimental & Theoretical Artificial Intelligence*, vol. 25, no. 4, pp. 527-542, 2013.

[28] B. Xue, M. Zhang, and W. N. Browne, "Particle swarm optimization for feature selection in classification: A multi-objective approach," *IEEE Transactions on Cybernetics*, vol. 43, no. 6, pp. 1656-1671, 2012.

[29] R. C. Eberhart and Y. Shi, "Particle swarm optimization: developments, applications and resources," *Proceedings of the 2001 Congress on Evolutionary Computation (IEEE Cat. No.01TH8546)*, pp. 81-86, 2001.

[30] S. Nanchian, A. Majumdar, and B. C. Pal, "Three-phase state estimation using hybrid particle swarm optimization," *IEEE Transactions on Smart Grid*, vol. 8, no. 3, pp. 1035-1045, 2015.

[31] Z. H. Zhan, J. Zhang, Y. Li, and H. S. H. Chung, "Adaptive particle swarm optimization," *IEEE Transactions on Systems, Man, and Cybernetics, Part B (Cybernetics)*, vol. 39, no. 6, pp. 1362-1381, 2009.

[32] F. Shahzad, S. Masood, and N. K. Khan, "Probabilistic opposition-based particle swarm optimization with velocity clamping," *Knowledge and information systems*, vol. 39, pp. 703-737, 2014.

Received 21 April 2024